Acta Pharmacologica Sinica

www.nature.com/aps

ARTICLE

Acquisition of taxane resistance by p53 inactivation in ovarian cancer cells

Changfa Shu[1,2], Xi Zheng[1,3], Alafate Wuhafu[1,4], Danielle Cicka[1], Sean Doyle[1], Qiankun Niu[1], Dacheng Fan[1], Kun Qian[1], Andrey A. Ivanov[1,5], Yuhong Du[1,5], Xiulei Mo[1] and Haian Fu[1,5,6]

Ovarian cancer is one of the most common gynecologic malignancies in women and has a poor prognosis. Taxanes are a class of standard first-line chemotherapeutic agents for the treatment of ovarian cancer. However, tumor-intrinsic and acquired resistance to taxanes poses major challenges to improving clinical outcomes. Hence, there is an urgent clinical need to understand the mechanisms of resistance in order to discover potential biomarkers and therapeutic strategies to increase taxane sensitivity in ovarian cancer. Here, we report the identification of an association between the TP53 status and taxane sensitivity in ovarian cancer cells through complementary experimental and informatics approaches. We found that TP53 inactivation is associated with taxane resistance in ovarian cancer cells, supported by the evidence from (i) drug sensitivity profiling with bioinformatic analysis of large-scale cancer therapeutic response and genomic datasets and (ii) gene signature identification based on experimental isogenic cell line models. Further, our studies revealed TP53-dependent gene expression patterns, such as overexpression of ACSM3, as potential predictive biomarkers of taxane resistance in ovarian cancer. The TP53-dependent hyperactivation of the WNT/β-catenin pathway discovered herein revealed a potential vulnerability to exploit in developing combination therapeutic strategies. Identification of this genotype-phenotype relationship between the TP53 status and taxane sensitivity sheds light on TP53-directed patient stratification and therapeutic discoveries for ovarian cancer treatment.

Keywords: Paclitaxel; Docetaxel; Ovarian cancer; TP53; ACSM3; WNT signaling

Acta Pharmacologica Sinica (2022) 43:2419–2428; https://doi.org/10.1038/s41401-021-00847-6

INTRODUCTION

Epithelial ovarian cancer (OC) is one of the most common ovarian malignancies and is the leading cause of mortality from gynecologic malignancies in the United States [1]. The asymptomatic nature of OC at early stages leads to poor prognosis and clinical outcomes [2]. Debulking surgery and systemic chemotherapy with cytotoxic agents are first-line standards of care for patients with advanced OC. However, because of the relapse rate of approximately 70%, it is an urgent but daunting task to improve the therapeutic benefit of OC treatments [3].

Taxanes, such as paclitaxel and docetaxel, are a class of diterpene compounds that are widely used as chemotherapeutic agents in OC treatment [3–5]. The primary mode of action of taxanes is to act as a molecular glue to hyperstabilize microtubules [6]. The antitumor activity of taxanes has been attributed to their interference with microtubule homeostasis, which is essential for cell cycle and DNA replication processes during mitosis [7, 8]. However, resistance to and relapse on taxanes have frequently been observed and significantly limit the impact of taxane-based therapeutic strategies for OC [9, 10].

The molecular mechanisms underlying taxane resistance have been explored across multiple tumor lineages in cancer cell line models [10–12]. Various mechanisms of resistance have been reported, such as overexpression of the multidrug transporter P-glycoprotein, aberrant drug metabolism, decreased sensitivity to death-inducing stimuli, and acquired mutations in the drug target [13–15]. However, predictive biomarkers of taxane sensitivity and combination therapeutic strategies remain to be developed.

Tumor protein 53 (TP53) is a well-known tumor suppressor that governs DNA repair and chromosomal integrity to keep DNA replication during mitosis in check [16, 17]. TP53-inactivating mutations have frequently been observed in many tumor types, including OC [18]. Given the important role of TP53 as a guardian of the genome, it is expected that the TP53 status is correlated with the response of cancer cells to taxane-based chemotherapy, which results in massive DNA damage and cellular stress [19]. However, the relationship between the TP53 status and taxane sensitivity is paradoxical and highly context-dependent [19–25], and delineation in a specific tumor context may be beneficial to tease apart the seemingly paradoxical correlations and identify tumor molecular subtypes suitable for targeted therapy.

Herein, to delineate the genotype-phenotype relationship between TP53 and taxane in the context of OC, we performed focused pharmacological studies using experimental isogenic

[1]Department of Pharmacology and Chemical Biology, Emory University School of Medicine, Atlanta, GA 30322, USA; [2]Department of Gynecology and Obstetrics, The Third Xiangya Hospital of Central South University, Changsha 410013, China; [3]Cancer Institute, the Second Affiliated Hospital, Zhejiang University School of Medicine, Hangzhou 310052, China; [4]The First Affiliated Hospital, Medical School of Xi'an Jiaotong University, Xi'an 710061, China; [5]Emory Chemical Biology Discovery Center, Emory University School of Medicine, Atlanta, GA 30322, USA and [6]Department of Hematology and Medical Oncology and Winship Cancer Institute, Emory University, Atlanta, GA 30322, USA
Correspondence: Haian Fu (hfu@emory.edu)

Received: 7 September 2021 Accepted: 20 December 2021
Published online: 14 January 2022

cancer cell line models coupled with unbiased bioinformatics analysis of a vast cellular therapeutic response and cancer genomic dataset. Our results have suggested that TP53 inactivation signatures are potential predictive biomarkers of taxane sensitivity and reveal TP53-dependent therapeutic vulnerabilities informing actionable combinatorial strategies.

MATERIALS AND METHODS

Cell lines

HEK293T embryonic kidney cells were purchased from American Type Culture Collection (ATCC) (Manassas, Virginia, USA) and cultured in Dulbecco's modified Eagle's medium (DMEM) (Millipore Sigma, Cat# 10-013-CV) (Burlington, Massachusetts, USA) supplemented with 10% fetal bovine serum (FBS) (Millipore Sigma, Cat# F0926) and 1× penicillin/streptomycin solution (Millipore Sigma, Cat# 30-001-CI). SKOV3 ovarian cancer cells were purchased from ATCC and cultured in McCoy's 5 A (modified) medium (Thermo Fisher, Cat# 16600108) (Waltham, Massachusetts, USA) supplemented with 10% FBS and 1× penicillin/streptomycin solution. Cells were cultured in a humidified incubator at 37 °C in 5% CO_2. Between passages, cells were washed with 1× PBS (Millipore Sigma, Cat# 21-040-CV) and were then detached by 0.25% trypsin with ethylenediaminetetraacetic acid (EDTA) (VWR, Cat# 45000–664)(Radnor, Pennsylvania, USA). All experiments were performed before passage 15. Cells were checked regularly for mycoplasma contamination by a MycoAlert Detection Kit (Lonza, Cat# LT07–318) (Quakertown, Pennsylvania, USA).

Analysis of differentially expressed genes (DEGs) associated with paclitaxel and docetaxel sensitivity

Differentially expressed gene (DEG) analysis was conducted with the limma package in R Studio as previously described [26, 27]. Briefly, according to the area under the curve (AUC) value of either paclitaxel or docetaxel from the CTRP database [28], the CCLE ovarian tissue samples were divided into 2 groups: a resistant group with high AUC values and a sensitive group with low AUC values. Genes with $|\log2FC| > 1$ and P-value < 0.05 were considered significantly upregulated or downregulated. All DEGs were visualized in a heatmap using the pheatmap package in R Studio.

Gene Set Enrichment Analysis (GSEA)

GSEA analyses were performed as described previously [27]. Briefly, the GSEABase package in R Studio was used to score the indicated gene sets from the hallmark molecular signature database as the reference gene sets. The rank of genes in the indicated pathways was used in accordance with the differential expression within either the resistance vs. sensitive or high expression vs. low expression groups. The normalized enrichment score (NES) was calculated to reflect the degree to which a set of genes was overrepresented at the extrema (top or bottom) across the entire ranked list. All GSEA analyses were performed strictly according to the instructions (https://www.bioconductor.org/packages/release/bioc/vignettes/GSEABase/inst/doc/GSEABase.pdf). For statistical significance, gene sets with $|NES| > 1$ and both a P value and false discovery rate (FDR) < 0.05 were considered significantly enriched. To gain more insight into the function of ACSM3, the TCGA OV database was downloaded from the GDC portal. All ovarian cancer samples were ranked according to the expression of ACSM3; DEGs were identified using the limma package in R Studio, and GSEA was then performed as described above.

Plasmids

Mammalian expression plasmids for TP53(WT) and TP53 mutants were generated as described previously [29]. TP53 mutations were introduced using a QuikChange Lightning Site-Directed Mutagenesis Kit (Agilent Technologies, Cat# 210518)(Santa Clara, California, USA). TP53(WT) and mutant cDNA sequences were cloned into the pHAGE lentiviral vector (a generous gift from Dr. Yiu Huen Tsang, Oregon Health & Science University) for lentiviral packaging. All plasmids were confirmed by FastDigest Bsp1407I (Thermo Scientific, Cat# FD0934) enzyme digestion and gene sequencing (GENEWIZ Sanger sequencing service)(South Plainfield, New Jersey, USA). The plasmids were purified using a QIAprep Spin Miniprep Kit (QIAGEN, Cat# 27106)(Germantown, Maryland, USA) or ZymoPURE™ Plasmid Maxiprep Kit (Zymo Research, Cat# D4203)(Irvine, California, USA).

Gene transfection

HEK293T cells at a confluence of 30%–40% were transfected with expression plasmids using 1 mg/mL polyethyleneimine (PEI) (Polysciences, Cat# 23966)(Warrington, Pennsylvania, USA) transfection reagent. A ratio of 3 μL of transfection reagent to 1 μg of plasmid DNA in a volume of 100 μL of Opti-MEM reduced-serum medium (Thermo Fisher, Cat# 31985070) was utilized for plasmid delivery. Transfection of SKOV3 cells was performed using FuGENE transfection reagent (Promega, Cat# E2312)(Madison, Wisconsin, USA) following the manufacturer's instructions. The expression of transfected genes was monitored by Western blotting with the corresponding antibodies.

Reagents

Paclitaxel (Selleckchem, Cat# S1150)(Houston, Texas, USA), docetaxel (Selleckchem, Cat# S1148), XAV939 (Cayman Chemical, Cat# 13596)(Ann Arbor, Michigan, USA), ICG001 (Cayman Chemical, Cat# 16257) and H151 (Cayman Chemical, Cat# 25857) were dissolved in dimethyl sulfoxide (Millipore Sigma, Cat# D2650–100 mL) and stored at −20 °C. WNT3A (R&D Systems, Cat# 5036-WN-010)(Minneapolis, Minnesota, USA) was dissolved in sterile PBS containing 0.1% bovine serum albumin (BSA) (Millipore Sigma, Cat# A9647) and stored at −80 °C.

Antibodies

Antibodies specific for the following proteins were used for immunoblotting: β-actin (Millipore Sigma, Cat# A5441, 1:5000 dilution), STING (Cell Signaling Technology, Cat# 13647, 1:1000 dilution)(Danvers, Massachusetts, USA), TBK1 (Cell Signaling Technology, Cat# 3504, 1:1000 dilution), phospho-TBK1 (S172) (Cell Signaling Technology, Cat# 5483, 1:1000 dilution), IRF3 (Abcam, Cat# ab68481, 1:1000 dilution)(Waltham, Massachusetts, USA), phospho-IRF3 (S386) (Abcam, Cat# 76493, 1:1000 dilution), ACSM3 (Santa Cruz Biotechnology, Cat# sc-377173, 1:400 dilution) (Dallas, Texas, USA), p53 (Cell Signaling Technology, Cat# 9282, 1:1000 dilution), anti-mouse IgG-HRP (Jackson ImmunoResearch, Cat# 115–035–003, 1:5000 dilution)(West Grove, Pennsylvania, USA) and anti-rabbit IgG-HRP (Jackson ImmunoResearch, Cat# 111–035–003, 1:5000 dilution).

Immunoblotting (Western blotting)

Cells were lysed in 1% NP-40 lysis buffer (1% NP-40, 20 mM Tris-HCl, 150 mM NaCl, 5% glycerol and 2 mM EDTA) containing freshly added protease inhibitor cocktail (Millipore Sigma, Cat# P8340), phosphatase inhibitor cocktail 2 (Millipore Sigma, Cat# P5726) and phosphatase inhibitor cocktail 3 (Millipore Sigma, Cat# P0044). Protein concentrations were measured by a BCA protein assay (Thermo Fisher, Cat# 23227) following the manufacturer's protocol. Proteins were heated for 5 min at 95 °C in 2× Laemmli buffer containing 200 mM DTT (Thermo Fisher, Cat# R0862). Alternatively, cells were directly lysed in 2× Laemmli buffer containing 200 mM DTT and heated for 30 min at 95 °C. Proteins were loaded on a 10% SDS-polyacrylamide gel and separated at a constant voltage of 150 V for 50 min using a Bio–Rad Mini-PROTEAN Tetra Cell. Proteins were then transferred from the gel to nitrocellulose

membranes (Bio–Rad, Cat# 1620112) (Berkeley, California, USA) using a Bio–Rad Mini Trans-Blot® Cell. The transfer system was operated at a constant voltage of 100 V for 120 min. Successful protein transfer was confirmed by checking protein markers (Thermo Fisher, Cat# 26616). Membranes were blocked with 5% nonfat milk in 1× TBS-T (20 mM Tris base, 150 mM sodium chloride, and 0.05% Tween 20; pH 7.6), except the membrane containing pIRF3-S386, which was blocked with 5% BSA in 1× TBS-T at room temperature for 1 h before overnight incubation at 4 °C with primary antibodies diluted in 1× TBS-T. After washing in 1× TBS-T three times for 10 min each at room temperature, membranes were incubated for 1 h at room temperature with HRP-conjugated secondary antibodies diluted in 1× TBS-T. Membranes were washed three times in 1× TBS-T, and SuperSignal™ West Pico PLUS Chemiluminescent Substrate (Thermo Fisher, Cat# 34580) was used to visualize immunoreactions in a Bio–Rad ChemiDoc Imaging System.

Quantitative real-time PCR (qRT–PCR)

Total RNA was isolated from cell lysates using an E.Z.N.A.® Total RNA Kit I (Omega, Cat# R6834–01)(Norcross, Georgia, USA) and digested with DNase I (Thermo Fisher, Cat# 18068–015). RNA concentrations were measured with an Epoch Microplate Spectrophotometer (BioTek, Santa Clara, California, USA). One microgram of total RNA was used for cDNA synthesis with a SuperScript™ III First-Strand Synthesis System (Thermo Fisher, Cat# 18080051) following the manufacturer's instructions. cDNA was diluted 1:5~1:10 in nuclease-free water, and qRT–PCR was performed using SYBR Green Supermix (Bio–Rad, Cat# 1725272) in a Mastercycler® RealPlex PCR System (Eppendorf, Enfield, Connecticut, USA). The following thermal cycling conditions were used for amplification of IFN-β: first step, 50 °C for 2′; second step, 95 °C for 10′; third step, 40 cycles at 94 °C for 10″, 59 °C for 30″, 72 °C for 45″ and 75 °C for 29″; fourth step, dissociation step [30]. For amplification of all other genes, the following thermal cycling conditions were used: first step, 95 °C for 2′; second step, 40 cycles at 95 °C for 15″, 60 °C for 15″ and 72 °C for 20″; third step, dissociation step. RNA expression was normalized to GAPDH expression. The data were subjected to comparative analysis of relative expression by the $2^{-\triangle\triangle Ct}$ method. All primers were ordered from Eurofins Genomics LLC. (Louisville, Kentucky, USA). The sequences of the primers used to amplify each gene were as follows: GAPDH (for: GAAGGTGAAGGTCGGAGT, rev: GAAGATGGTGATGGGATTTC), IFIT1 (for: TTGATGACGATGAAATGCC TGA, rev: CAGGTCACCAGACTCCTCAC), IFNβ (for: CGCCGCATTGACC ATCTA, rev: GACATTAGCCAGGAGGTTCTCA), CXCL10 (for: GTGGCA TTCAAGGAGTACCTC, rev: TGATGGCCTTCGATTCTGGATT), ACSM3 (for: AGGAAGATGCTACGTCATGCC, rev: ATCCCCAGTTTGAAGTCCT GT), β-Catenin (for: TCTCCTCAGATGGTGTCTGCT, rev: TTACCCAAG CATTTTCACCAG), AXIN2 (for: ACAACAGCATTGTCTCCAAGCAGC, rev: GCGCCTGGTCAAACATGATGGAT), MMP7 (for: GGGATTAACTTCCTG TATGC, rev: GATCTCCATTTCCATAGGTTG), and PCNA (for: GCGTGA ACCTCACCAGTATGT, rev: TCTTCGGCCCTTAGTGTAATGAT).

Transcriptome (RNA-seq) analysis

The transcriptomes of SKOV3 TP53 isogenic cells were analyzed by mRNA sequencing (Novogene Corporation Inc., Sacramento, California, USA) using Illumina TruSeq technology. Briefly, total RNA from SKOV3 cells was isolated from cell lysates using an E.Z.N.A.® Total RNA Kit I. RNA sequence reads were aligned to the human reference genome (GRCh38). Genes were considered to be significantly up- or downregulated when the adjusted *P* value was < 0.05. Gene ontology enrichment analysis was performed at Metascape [31]

shRNA knockdown

To knock down endogenous human ACSM3, shRNAs were purchased from a commercial source, namely, the MISSION shRNA library (Millipore Sigma). The information for each shRNA was as follows: ACSM3-shRNA1, TRCN0000083241; ACSM3-shRNA2: TRCN 0000419608. A nontargeting shRNA (Millipore Sigma, Cat# SHC 016–1EA) was used as the control. shRNAs were packaged into lentiviruses and transduced into target cells. For transduction, target cells were incubated with lentivirus-containing supernatants for 48 h and were then selected with the appropriate concentration (2 μg/mL) of puromycin (InVivoGene, Cat# ant-pr-1) (San Diego, California, USA). The targeting efficiency was evaluated by immunoblotting.

Generation of lentiviral particles

HEK293T cells (5×10^6) were seeded into a 6-well plate and transfected using PEI transfection reagent with 2 mg of the lentiviral expression vector together with 1.6 mg of pCMV-dR8.91 and 0.66 mg of pCMV-VSVG (a generous gift from Emory University Viral Vector Core). After 48 to 72 h of transfection, the medium containing lentiviral particles was collected and centrifuged at 4 °C and 3000 r/min for 15 min. Then, the medium was filtered through a 0.45 mM PVDF filter (Millipore Sigma, Cat# SLHV033RS) and stored at −80 °C.

Cell viability assay

Cell viability was measured by CellTiter-Blue reagent (Promega, Cat# G8081) following the manufacturer's protocol, as previously described [32]. Briefly, CellTiter-Blue was added to each well and incubated until the signal increased to the linear range. The fluorescence intensity of each well was measured in a PHERAstar FSX multimode plate reader (Ex 545 nm, Em 615 nm; BMG LABTECH)(Cary, North Carolina, USA). Wells containing medium alone were used as blank controls for background correction.

Colony formation assay

The colony formation assay was performed as we described previously [27]. Briefly, cells (in suspension) were plated in 6-well plates at a density of 2000~4000 cells per well. On the second day, cells were treated with DMSO or 2.5 nM paclitaxel. Every 3 days, the medium was replaced with fresh medium containing the corresponding agent. After a 15-day treatment, the medium was removed, and cell colonies were stained with crystal violet. Images were acquired using a ChemiDoc Touch Imaging System (Bio–Rad), and colony areas were quantified using the ImageJ Colony Area plugin [33].

IncuCyte-based apoptosis assay

Cells were seeded in 96-well plates (Millipore Sigma, Cat# 3603) or 384-well plates (Millipore Sigma, Cat# 3764) overnight. The next day, medium with the indicated agents and IncuCyte® Caspase-3/7 Green Dye (Sartorius, Cat# 4440; 1:1000 dilution, final concentration of 5 μM)(Ann Arbor, Michigan, USA) was added. The plates were put into an IncuCyte® S3 Live-Cell Analysis System. Cells were then subjected to phase contrast and green fluorescence imaging every 2 h. The results were analyzed by the corresponding software.

Luciferase reporter assay

SKOV3 cells were seeded in 6-well plates. The next day, the cells were transfected with VF plasmids along with the firefly luciferase TCF/LEF plasmid (Promega, Cat# E4611) and Renilla luciferase plasmid, which served as the internal control. Cells were treated with either WNT3A (R&D Systems, Cat# 5036-WN-010) or PBS containing 0.1% BSA as the control, as indicated, before collection. Then, cells were collected and resuspended in PBS. Twenty microliters of the cell suspension was transferred to a 384-well plate (Millipore Sigma, Cat# 3705), and a TCF/LEF reporter assay was performed using a Dual-Glo luciferase kit (Promega, Cat# E2920) following the manufacturer's instructions. The firefly luciferase signal was normalized to the control Renilla luciferase signal.

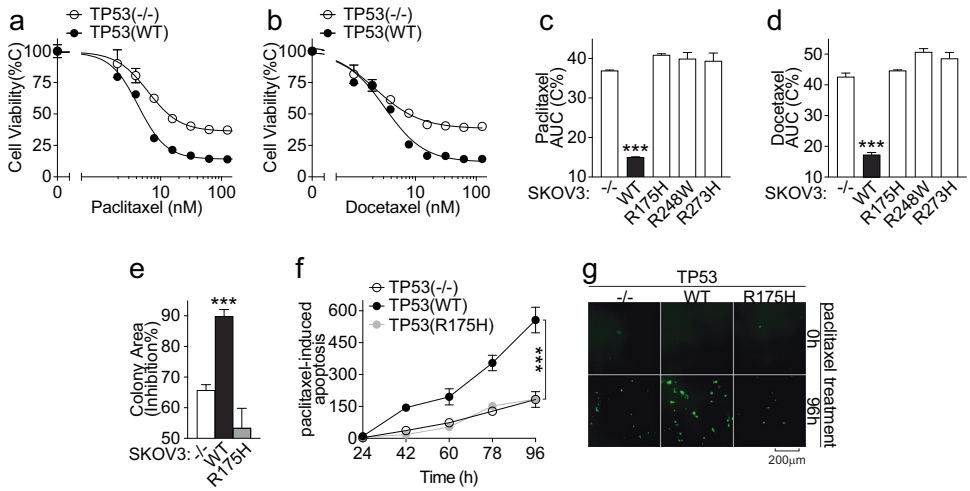

Fig. 1 Identification of the association between taxane resistance and TP53 inactivation in ovarian cancer cells. a–b Dose–response curve of isogenic SKOV3 cells in response to paclitaxel (**a**) and docetaxel (**b**). Parental SKOV3 cells with TP53 deletion (−/−) and their isogenic TP53 wild-type (WT) reconstituted counterparts were treated with different concentrations of paclitaxel and docetaxel as indicated. The cellular response to taxane treatment was evaluated by a cell viability assay and quantified by normalization to the viability percentage in DMSO control cells. The data are presented as the mean±SD of three independent experiments. **c–d** Bar graph showing taxane sensitivity in isogenic SKOV3 cells in response to paclitaxel (**c**) and docetaxel (**d**). Parental SKOV3 cells with TP53 deletion (−/−) and their isogenic counterparts reconstituted with wild-type (WT) TP53 or TP53 carrying an inactivating missense mutation (R175H, R248W, or R273H) were treated with different concentrations of paclitaxel and docetaxel. The cellular response to taxane treatment was evaluated by a cell viability assay and quantified as the areas under the dose–response curve (AUC) values. The results are presented as the mean±SD of three independent experiments. ***$P \le 0.001$. **e** Bar graph showing taxane sensitivity in terms of colony formation in isogenic SKOV3 cells in response to paclitaxel. Parental SKOV3 cells with TP53 deletion (−/−) and their isogenic counterparts reconstituted with wild-type TP53 (WT) or TP53 carrying the inactivating R175H mutation were treated with paclitaxel (2.5 nM). The cellular response to paclitaxel treatment was evaluated by a colony formation assay and quantified by the colony area. The results are presented as the mean±SD of the percentage of inhibition (% Inhibition) from three independent experiments. ***$P \le 0.001$. **f** Time curve showing paclitaxel-induced apoptosis. Parental SKOV3 cells with TP53 deletion (−/−) and their isogenic counterparts reconstituted with wild-type (WT) TP53 or TP53 carrying the inactivating R175H mutation were treated with paclitaxel (5 nM). Apoptosis was monitored in real-time by a Caspase3/7 fluorogenic reporter assay. The results are presented as the mean±SD of the percentage of the number of fluorescence-positive cells from three independent experiments. ***$P \le 0.001$. **g** Representative fluorescence images showing paclitaxel-induced apoptosis as described in (**f**) at the indicated time points

Statistical analysis

All analyses were performed using GraphPad Prism version 7.0 (GraphPad Software, La Jolla, California, USA). The dose-dependent induced cancer cell growth inhibition curve was generated using GraphPad Prism based on a sigmoidal dose–response (variable slope) equation. Statistical significance was assessed using unpaired two-tailed Student's *t* test or one-way ANOVA followed by Tukey's *post-hoc* test. *P* values < 0.05 were considered statistically significant.

RESULTS

TP53 inactivation is associated with taxane resistance in isogenic ovarian cancer cells

Taxanes, such as paclitaxel and docetaxel, are first-line chemotherapeutic agents for ovarian cancer treatment [3, 34]. However, primary and acquired resistance to taxanes present a daunting challenge to improving therapeutic outcomes of ovarian cancer [35]. Identification of predictive biomarkers of taxane sensitivity is an urgent clinical need for patient stratification. Although previous studies indicated that the status of tumor protein 53 (TP53) might be associated with taxane sensitivity in ovarian cancer, the context-dependent paradoxical observations warrant further investigation [22, 24, 25].

To determine the association between the TP53 status and taxane sensitivity in the ovarian cancer context, we first compared cell viability in response to paclitaxel and docetaxel using a panel of representative isogenic SKOV3 cells with a matched genetic background. At the basal level, we did not observe a significant difference in cell proliferation between the parental SKOV3 cells with TP53 deletion (−/−) and the TP53 wild-type (WT) isogenic cells (Supplementary Fig. 1). Upon taxane treatment, we found that the TP53(−/−) cells responded dose-dependently to paclitaxel, with a GI_{50} (half-maximal cell growth inhibitory concentration) of 12.9 ± 1.1 nM, whereas the WT counterparts exhibited a significantly lower GI_{50} of 5.4 ± 0.7 nM ($P \le 0.001$) (Fig. 1a). A similar association was observed between the TP53 status and cell viability in response to docetaxel treatment (Fig. 1b). The areas under the curve (AUCs) of the dose–response curves showed significantly decreased AUC values in the TP53(−/−) cells compared to the parental TP53(−/−) control cells (Fig. 1c, d), suggesting TP53(WT)-associated acquisition of taxane sensitivity. In contrast, there was no significant difference in taxane sensitivity, in terms of the AUC value, between TP53(−/−) cells and other isogenic cells carrying *TP53*-inactivating mutations, such as R175H, R248W and R273H (Fig. 1c, d). Moreover, we observed a similar TP53 status-dependent response with long-term paclitaxel treatment in the colony formation assay (Fig. 1e). Altogether, these results suggested that inactivation of TP53 is associated with resistance to taxane-induced growth inhibition in ovarian cancer cells.

Taxane-induced growth inhibition has been shown to be mediated in part through apoptosis[21]. To further determine the association between the TP53 status and taxane sensitivity, we next compared paclitaxel-induced apoptosis between isogenic SKOV3 cells. We found that paclitaxel treatment led to significantly more apoptotic cells in terms of caspase3/7 activity in TP53(WT) cells than in their (−/−) and R175H isogenic counterparts (Fig. 1f, g). These results suggested a potential impairment of the apoptotic machinery underlying paclitaxel resistance in TP53-inactivated cells.

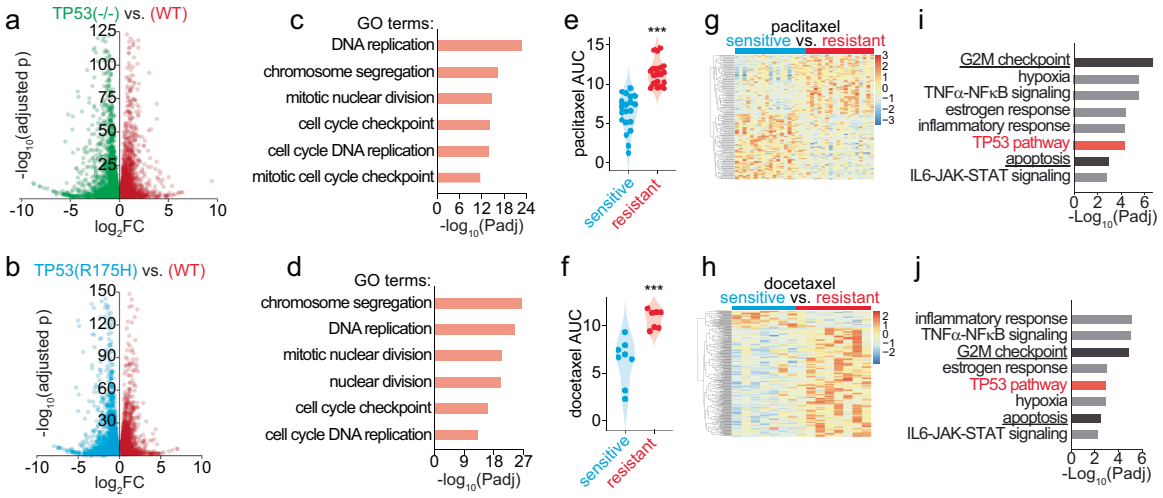

Fig. 2 Informatic analysis of differentially expressed genes (DEGs) associated with the TP53 status and taxane sensitivity in ovarian cancer cells. a–b Volcano plots showing the identification of DEGs by comparing mRNA expression in isogenic SKOV3 TP53(WT) cells, TP53 deletion (−/−) cells (**a**) and TP53-inactivate (R175H mutation) cells (**b**). The data are presented as the average gene expression levels from technical triplicates. **c–d** Bar graph showing the top enriched GO terms for TP53(WT)-associated upregulated DEGs. **e–f** Violin plot showing the classification of taxane-sensitive and taxane-resistant ovarian cancer cells according to the area under the curve values of the dose–response viability curves of ovarian cancer cells in response to paclitaxel (**e**) and docetaxel (**f**) using the median AUC value based on the CTRP database as the cutoff. **g–h** Heatmap of the gene expression matrix between paclitaxel-sensitive/resistant (**g**) and docetaxel-sensitive/resistant (**h**) ovarian cancer cells. **i–j** Bar graph showing the representative pathways enriched with paclitaxel (**i**) and docetaxel (**j**) sensitivity-associated DEGs, as determined by GSEA

Recently, the stimulator of interferon genes (STING)-dependent apoptotic machinery has been suggested to be involved in paclitaxel-induced growth inhibition [36]. To determine the involvement of STING, we compared paclitaxel-induced STING-dependent pathway activation between isogenic SKOV3 cells. We found that paclitaxel significantly activated STING-dependent signaling in TP53(WT) cells but not in their (−/−) and R175H isogenic counterparts in terms of the phosphorylation of the downstream STING effectors TBK1 and IRF3 (Supplementary Fig. 2a) and the mRNA expression of the IRF3 target genes IFIT1, IFNβ and CXCL10 (Supplementary Fig. 2b). In support of this finding, the taxane-induced growth inhibition of TP53(WT) cells was partially abolished by additional treatment with the STING antagonist H151 (Supplementary Fig. 2c, d). These results suggested that TP53 inactivation leads to taxane resistance in ovarian cancer cells in part through impaired STING-dependent apoptotic signaling.

TP53-dependent signature genes are associated with taxane sensitivity in ovarian cancer cells

TP53 is a well-known transcription factor that regulates the expression of many genes to suppress tumor growth [37]. Given the potential association between the TP53 status and taxane sensitivity, we reasoned that there might be similar associations between TP53 target genes and taxane sensitivity. To test this hypothesis and identify TP53-dependent signature genes involved in shaping taxane sensitivity, we performed RNAseq to experimentally define a TP53 target gene set, coupled with parallel informatics analysis of large-scale cancer cell line taxane sensitivity and transcriptome datasets from the Cancer Therapeutic Response Portal (CTRP) [28].

To define TP53-dependent gene expression in ovarian cancer cells, we first compared the differentially expressed genes (DEGs) between isogenic SKOV3 cells. From the RNAseq analysis, we found a diverse array of DEGs between isogenic SKOV3 cells with different TP53 statuses (Fig. 2a, b). For example, analysis of DEGs identified more than 3000 genes that were significantly up- or downregulated in TP53(WT) cells compared to their isogenic (−/−) and R175H counterparts. Gene Ontology analysis revealed that the TP53(WT)-associated upregulated DEGs were mostly enriched in pathways that are critical for DNA integrity and cell cycle regulation (Fig. 2c, d), supporting the known biological function of TP53 as a master regulator of the DNA damage response [38]. These results not only confirmed the TP53 dependency of these isogenic ovarian cancer cells at the transcriptome level but also identified a solid set of experimentally determined TP53-dependent DEGs for further analysis.

In parallel, to identify potential biomarkers of taxane sensitivity, we analyzed the DEGs between taxane-sensitive and taxane-resistant ovarian cancer cells. From analysis data for a panel of tested ovarian cancer cells in the CTRP, we first classified the cells into sensitive and resistant groups based on their responses to paclitaxel and docetaxel in terms of the AUC values calculated from the drug dose–response cell viability curves (Fig. 2e, f). The significant differences between the sensitive and resistant groups in terms of the AUC values (Fig. 2e, f) and gene expression matrix (Fig. 2g, h) in turn confirmed the validity of this classification strategy. By analysis of the DEGs with the selected statistical cutoff, we identified 84 (254) upregulated and 93 (39) downregulated DEGs in paclitaxel (docetaxel)-resistant cells compared to sensitive cells. GSEA revealed that these taxane sensitivity-associated DEGs were significantly enriched in cell cycle regulation and apoptosis pathways, supporting the known mode of action of taxanes [39] (Fig. 2i, j). In addition, these analysis results revealed many genes enriched in other pathways, such as tumor necrosis factor (TNF) signaling and inflammatory response, which may potentially correlate with taxane sensitivity and thus warrant further investigation.

From this unbiased CTRP dataset analysis, we also found that some taxane sensitivity-related DEGs were significantly enriched in TP53-dependent pathways (Fig. 2i, j). These results further independently confirmed our previous experimental discovery of the association between the TP53 status and taxane sensitivity in additional patient-derived ovarian cancer cell lines with diverse genetic backgrounds. To further identify TP53-dependent signature genes that may be associated with taxane sensitivity, we intersected the set of TP53-dependent DEGs experimentally defined in isogenic cells with the set of taxane sensitivity-

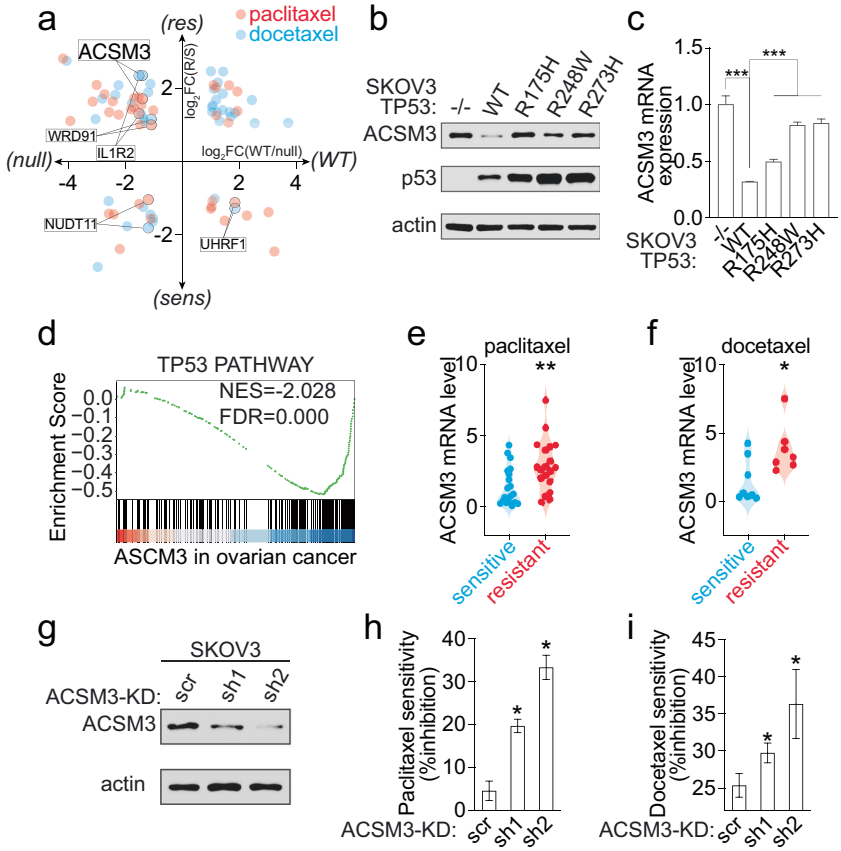

Fig. 3 Identification of the association between TP53-dependent ACSM3 expression and taxane sensitivity in ovarian cancer cells. **a** Scatter plot showing the correlations between the TP53 status and the taxane sensitivity-associated DEGs shown in Fig. 2. **b** Representative immunoblot showing overexpression of the ACSM3 protein in TP53-inactivated ovarian cancer cells. Cell lysates from parental SKOV3 cells with TP53 deletion (−/−) and their isogenic counterparts reconstituted with wild-type (WT) TP53 or TP53 carrying an inactivating missense mutation (R175H, R248W, or R273H) were analyzed by SDS–PAGE and Western blotting with the indicated antibodies. **c** Bar graph showing overexpression of ACSM3 mRNA in TP53-inactivated ovarian cancer cells. ACSM3 mRNA expression in parental SKOV3 cells with TP53 deletion (−/−) and their isogenic counterparts reconstituted with wild-type (WT) TP53 or TP53 carrying an inactivating missense mutation (R175H, R248W, or R273H) were analyzed by qPCR. The data are presented as the means±SDs of normalized mRNA expression levels from three independent experiments. ***$P \le 0.001$. **d** Enrichment plot showing the association of ACSM3 expression and TP53 pathway gene expression in ovarian cancer patient samples from TCGA. **e**–**f** Violin plots showing the association between ACSM3 mRNA expression and taxane sensitivity. The ACSM3 mRNA expression levels in paclitaxel-sensitive/resistant (**e**) and docetaxel-sensitive/resistant (**f**) cells were identified by analysis of the CTRP database. *$P \le 0.05$, **$P \le 0.01$. **g** Representative immunoblot showing shRNA-mediated knockdown (KD) of ACSM3 in SKOV3 cells. Cell lysates from two isogenic ACSM3 knockdown cell lines (sh1: shRNA1; sh2: shRNA2) and scrambled (scr) shRNA control cells were analyzed by SDS–PAGE and Western blotting with the indicated antibodies. **h**–**i** Bar graphs showing increased taxane sensitivity in ACSM3-KD cells. SKOV3 cells expressing WT ACSM3 (scr) or with shRNA-mediated ACSM3 knockdown (sh1 and sh2) were treated with paclitaxel (**h**, 5 nM) and docetaxel (**i**, 2.5 nM) for three days. Taxane sensitivity was evaluated by a cell viability assay. The results are presented as the mean±SD of the percentage of inhibition (%Inhibition) from three independent experiments. *$P \le 0.05$

associated DEGs computationally defined from CTRP dataset analysis (Fig. 3a). From this intersection, we identified five potential signature genes whose expression was significantly correlated with TP53 status and sensitivity to both paclitaxel and docetaxel in ovarian cancer cells (Fig. 3a). These five candidate genes were ACSM3 (Acyl-CoA Synthetase Medium Chain Family Member 3), IL1R2 (Interleukin 1 Receptor Type 2), NUDT11 (Nudix Hydrolase 11), UHRF1 (Ubiquitin like with PHD and Ring Finger Domains 1) and WDR91 (WD Repeat Domain 91). Altogether, these results revealed TP53-dependent gene candidates as potential biomarkers for predicting the therapeutic response to taxanes.

TP53-dependent ACSM3 expression is negatively correlated with paclitaxel sensitivity in ovarian cancer cells

To further confirm the association between the TP53 status and taxane sensitivity, we next prioritized potential biomarker candidates from the above analysis to determine whether their gene expression is indeed TP53 dependent and also correlates with taxane sensitivity. ACSM3 was identified as such a potential biomarker; its expression was suggested to be upregulated in TP53-inactivated cells by RNAseq profiling and to correlate with taxane resistance in ovarian cancer cells by CTRP analysis (Fig. 3a).

To determine the relationship between ACSM3 and TP53, we performed additional experimental and informatics studies. First, we found that the ACSM3 protein and mRNA levels were significantly decreased in TP53(WT) cells compared to the isogenic TP53-inactivated SKOV3 cells (Fig. 3b, c). Furthermore, GSEA showed a negative enrichment score between TP53 pathway genes and ACSM3 expression, suggesting that ACSM3 mRNA expression was negatively correlated with TP53 activation in ovarian cancer patient samples (Fig. 3d). These results from both experimental and informatics studies confirmed that ACSM3 expression is indeed TP53-dependent.

By CTRP dataset analysis, we found that ACSM3 was over-expressed in taxane-resistant ovarian cancer cells (Fig. 3e, f). To confirm this correlation, we tested taxane sensitivity in isogenic

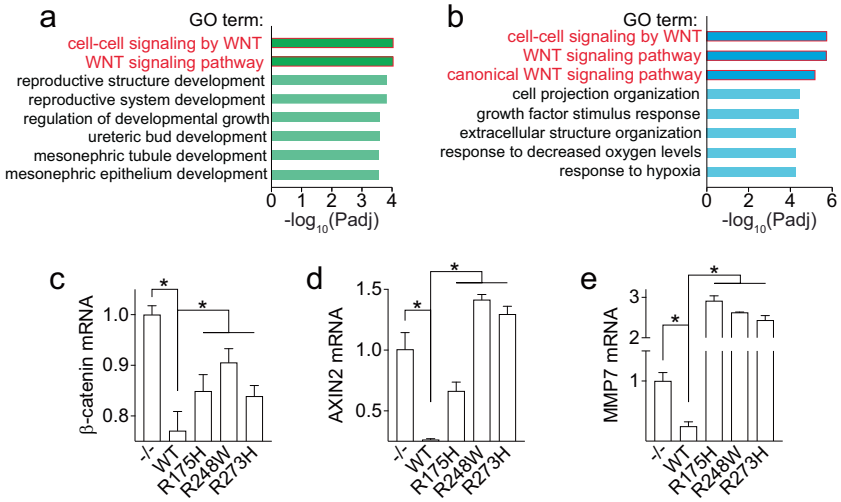

Fig. 4 Upregulation of WNT/β-catenin signaling in TP53-inactivated ovarian cancer cells. a–b Bar graphs showing the GO terms enriched with TP53(−/−)-associated (**a**) and TP53(R175H)-associated (**b**) upregulated DEGs. **c–e** Bar graphs showing upregulation of WNT/β-catenin pathway and target gene expression at the basal level, including β-catenin (**c**), AXIN2 (**d**), and MMP7 (**e**) expression, in TP53-inactivated isogenic SKOV3 cells. mRNA levels in parental SKOV3 cells with TP53 deletion (−/−) and their isogenic counterparts reconstituted with wild-type (WT) TP53 or TP53 carrying an inactivating missense mutation (R175H, R248W, or R273H) were analyzed by qPCR. The data are presented as the means ± SDs of relative mRNA expression levels from three independent experiments. *$P \leq 0.05$

SKOV3 cells via ACSM3-targeted genetic loss-of-function studies (Fig. 3g). We found that the parental SKOV3 cells with high ACSM3 expression were resistant to paclitaxel, whereas the isogenic cells with ACSM3 knockdown developed significantly increased sensitivity to paclitaxel and docetaxel (Fig. 3h, i). Thus, using ACSM3 as an example, we confirmed that ACSM3 expression is TP53-dependent and correlates with taxane sensitivity. These results not only suggest TP53-dependent ACSM3 expression as a potential biomarker to predict the response of ovarian cancer to taxane but also provide evidence to further support the association between the TP53 status and taxane sensitivity in ovarian cancer.

TP53-dependent activation of the WNT/β-catenin pathway informs a combination strategy to improve taxane sensitivity

By a series of experimental and informatics confirmatory studies, we demonstrated that taxane resistance is correlated with TP53 inactivation and revealed potential TP53-dependent genes as biomarkers for taxane sensitivity prediction in ovarian cancer cells. However, therapeutic strategies to improve taxane sensitivity in TP53-inactivated cells remain to be explored.

To identify potential collateral therapeutic vulnerabilities with TP53 inactivation in ovarian cancer cells, we revisited the TP53-dependent DEGs from our previous RNA-seq analysis (Fig. 2a, b). From the gene ontology analysis, we found that WNT signaling pathway was one of the GO terms most significantly enriched with upregulated DEGs in TP53-mutated cells compared to WT cells (Fig. 4a, b). Indeed, we found that TP53-inactivated cells had significantly higher mRNA expression levels of WNT pathway genes, such as β-catenin (Fig. 4c), and WNT target genes, such as AXIN2 and MMP9 (Fig. 4d, e), suggesting potential Wnt signaling hyperactivation in TP53-inactivated cells. In addition, multiple pharmacological inhibitors targeting WNT signaling are available and are under evaluation in clinical trials [40]. Considering these observations collectively, we hypothesized that activation of WNT signaling is associated with the TP53 status, while pharmacological inhibition of hyperactivated WNT signaling could be a potential therapeutic strategy to overcome taxane resistance in TP53-inactivated ovarian cancer cells.

To test our hypothesis, we first sought to determine whether WNT/β-catenin signaling activation is associated with the TP53 status. Using a TCF/LEF (T cell factor and lymphoid enhancer factor)-based luciferase reporter assay, we compared WNT-induced β-catenin transcriptional activity between isogenic SKOV3 cells. We found that WNT3A stimulation resulted in a significantly higher β-catenin-TCF/LEF luciferase signal in TP53-inactivated cells than in their isogenic WT counterparts (Fig. 5a). Similarly, WNT3A stimulation induced significant increases in the mRNA expression of β-catenin target genes, such as MMP7, AXIN2 and PCNA, in TP53-inactivated cells compared to their isogenic WT counterparts (Fig. 5b–d). Interestingly, we found that ACSM3 protein expression was also significantly increased upon WNT3A stimulation in TP53 (−/−) and TP53(R175H) SKOV3 cells but not in the WT isogenic counterpart (Fig. 5e), indicating that TP53-dependent ACSM3 expression might be regulated in part through aberrant WNT signaling in ovarian cancer cells with TP53 inactivation. These results suggested that WNT signaling is hyperactivated in TP53-inactivated ovarian cancer cells, independently supporting the previously reported hyperactivation of WNT signaling by TP53 inactivation [41, 42].

Hyperactivation of WNT/β-catenin signaling is frequently observed in cancer [43, 44], and a panel of WNT pathway-targeted pharmacological agents have been developed for therapeutic development [40]. Given the observed hyperactivation of WNT signaling in TP53-inactivated ovarian cancer cells, which are taxane-resistant, we reasoned that pharmacological inhibition of the WNT pathway may constitute a potential combination strategy to improve taxane sensitivity in ovarian cancer. To test this hypothesis, we examined the viability of ovarian cancer cells in response to taxane treatment in combination with ICG001 or XAV939, two known WNT pathway inhibitors [45, 46]. We found that TP53(−/−) SKOV3 ovarian cancer cells, which are resistant to paclitaxel treatment (GI_{50} = 12.9 ± 1.1 nM), exhibited significantly increased sensitivity to paclitaxel, with GI_{50} values of 0.25 ± 0.07 and 0.19 ± 0.07 nM in combination with ICG001 and XAV939, respectively (Supplementary Fig. 3a, b). These results suggest that pharmacological inhibition of hyperactivated WNT signaling may be a potential combination strategy for taxane-based chemotherapy in TP53-inactivated ovarian cancer cells.

Altogether, the results of our studies suggested that TP53 inactivation is associated with the acquisition of resistance to taxane-based chemotherapy in ovarian cancer cells. Unbiased

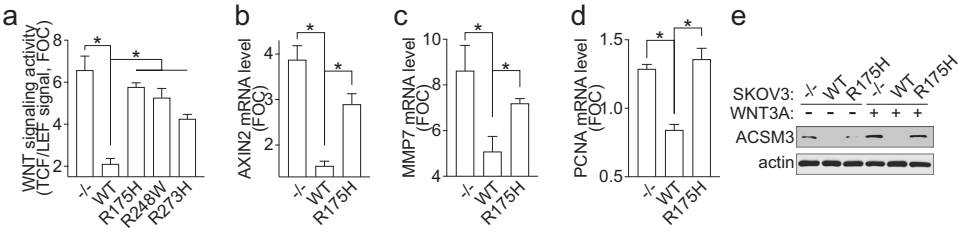

Fig. 5 Targeting of overactivated WNT/β-catenin signaling in TP53-inactivated ovarian cancer cells to improve taxane sensitivity. a Bar graph showing overactivation of WNT/β-catenin signaling induced by WNT3A. WNT/β-catenin signaling activity was measured by a TCF/LEF luciferase reporter assay using parental SKOV3 cells with TP53 deletion (−/−) and their isogenic counterparts reconstituted with TP53 wild-type (WT) or TP53 carrying an inactivating missense mutation (R175H, R248W, or R273H) that were treated with WNT3A (100 ng/mL) for 24 h. Differences were quantified as the fold change (FC) in the luciferase signal upon WNT3A stimulation, and the data are presented as the mean ± SD of three independent experiments. *$P \le 0.05$. **b**–**d** Bar graphs showing overactivation of the WNT/β-catenin pathway in terms of the expression of target genes, including AXIN2 (**b**), MMP7 (**c**), and PCNA (**d**), in TP53-inactivated isogenic SKOV3 cells upon WNT3A stimulation. mRNA levels in parental SKOV3 cells with TP53 deletion (−/−) and their isogenic counterparts reconstituted with wild-type (WT) TP53 or TP53 carrying an inactivating missense mutation (R175H) upon WNT3A (100 ng/mL) stimulation for 24 h were analyzed by qPCR. Differences were quantified as the fold change (FC) in the mRNA expression level upon WNT3A stimulation, and data are presented as the mean±SD of three independent experiments. *$P \le 0.05$. **e** Representative Western blot showing WNT3A-dependent ACSM3 expression in TP53-inactivated ovarian cancer cells. Cell lysates from parental SKOV3 cells with TP53 deletion (−/−) and their isogenic counterparts reconstituted with wild-type (WT) TP53 or TP53 carrying an inactivating missense mutation (R175H) upon WNT3A (100 ng/mL) stimulation for 24 h were analyzed by SDS–PAGE and Western blotting with the indicated antibodies

molecular profiling identified TP53-dependent gene expression patterns as potential predictive biomarkers of taxane sensitivity, further supporting the association between the TP53 status and taxane responsiveness. Furthermore, our results suggested hyperactivation of WNT signaling as a collateral vulnerability upon TP53 inactivation, providing potential therapeutic insight into the use of WNT pathway inhibitors as combination agents to improve the response to taxane-based chemotherapy in resistant TP53-inactivated ovarian cancer cells.

DISCUSSION

Taxane-based chemotherapy is a first-line therapeutic regimen for various cancers, including ovarian, breast and lung cancers [3, 47, 48]. However, the common occurrence of resistance and relapse presents an unmet clinical need to improve therapeutic outcomes. Despite previous dispersed efforts to identify potential predictive biomarkers of taxane sensitivity, the diverse underlying molecular mechanisms reported in various cancer types implied that there is no "one-size-fits-all" mechanism, a possibility that warrants further investigation in a context-specific manner. In this study, we focused on the context of OC and performed pharmacological and bioinformatics studies to identify the potential biomarkers associated with taxane sensitivity. Our results in OC-relevant experimental cell line models suggested a significant association between a TP53 inactivation status and taxane resistance. Moreover, our studies revealed several TP53-dependent genes, such as ACSM3, as potential biomarkers and revealed hyperactivated WNT signaling as a collateral vulnerability for developing drug combination regimens. Our OC-oriented in vitro cell line model studies added a critical piece of evidence supporting the genotype-phenotype relationship between the TP53 pathway status and the taxane response, which needs further investigation in relevant in vivo ovarian cancer models.

The genotype-phenotype relationship between the TP53 status and the taxane response is controversial and context-specific. Our results support an association between TP53 inactivation and taxane resistance in OC cells. Similar associations between taxane resistance and TP53 genetic deletion or loss-of-function mutation have been observed in previous studies using OC [25] and non-small-cell lung cancer cell models [23]. In contrast, some studies have suggested that a TP53(WT) status is either associated with or independent of taxane resistance [20–22]. For example, an early study using nine OC cell lines did not find statistically significant evidence indicating that genetic alterations in TP53 at the DNA level are surrogate markers for paclitaxel sensitivity [20]. In our CTRP dataset analysis, although the correlations between taxane sensitivity and TP53 genetic mutation at the DNA level across a panel of ovarian cancer cells were still not statistically significant (data not shown), we found that TP53 pathway gene expression patterns representing the TP53 activation status at the transcriptome level were significantly correlated with taxane sensitivity (Fig. 2i, j). This discrepancy in the correlation between the TP53 genetic status at the DNA level and the TP53 pathway activation status at the transcriptome level could be explained by the documented intricate posttranscriptional mechanisms regulating TP53(WT) [49]. These results suggest that the identification of signature genes representing the TP53 activation status, in addition to TP53 genetic alterations, may be an alternative approach to define biomarkers of taxane sensitivity in OC and other cancer types.

TP53 is a known tumor suppressor that acts as "the guardian of the genome" primarily through its pluripotent transcription factor activity in inducing the transcription of genes that control numerous biological functions and cell fates, such as DNA replication, cell cycle progression and apoptosis [38]. Upon TP53 activation in response to cellular stress, TP53 binds as a tetramer to the consensus sequence RRRCWWGYYY (R = A/G, W = A/T, Y = C/T) in the regulatory regions of its target genes [50]. Although consensus sequence-based genome-wide analyses have suggested hundreds to thousands of potential candidate TP53 target genes [51], experimental validation of these candidates is indispensable for understanding TP53 biology in a cancer-specific context. In our study, we identified an OC-directed TP53-dependent gene signature using isogenic SKOV3 ovarian cancer cells with a matched genetic background. This experimentally determined TP53-dependent gene set not only confirmed the known biological function of TP53 in regulating DNA replication and cell cycle progression (Fig. 2c, d) but also can serve as a valuable resource for future in-depth investigation of novel aspects of TP53 biology in the ovarian cancer context.

ACSM3 is a subunit of CoA ligases that produce acyl-CoA by interacting with medium-chain fatty acids on the outer mitochondrial membrane [52]. It has been demonstrated that loss of ACSM3 expression promotes metastasis and predicts poor prognosis in hepatocellular carcinoma and OC, suggesting that ACSM3 performs a tumor suppressor function during tumorigenesis and cancer progression [53, 54]. However, how ACSM3 is regulated and the function of ACSM3 in shaping the chemotherapeutic

response are largely unknown. Here, our results showed that ACSM3 was overexpressed in TP53-inactivated cells (Fig. 3a–c) and that genetic loss-of-function perturbation of ACSM3 improved taxane sensitivity in TP53-inactivated OC cells (Fig. 3g–i). These results implied that low ACSM3 expression, coupled with the TP53 (WT) genotype, may be a potential biomarker for OC patient stratification toward personalized taxane-based chemotherapy.

The WNT signaling pathway is a key pathway that regulates cancer cell stemness and metastasis [44]. Aberrant activation of WNT signaling has been reported in multiple cancer types, including ovarian cancer [43]. In our study, we found that in ovarian cancer cells, WNT signaling was inhibited by TP53 activation, whereas hyperactivation of WNT signaling was associated with TP53 inactivation, suggesting crosstalk between the WNT and TP53 pathways. Similar crosstalk has also been reported in colorectal cancer cells and mechanistically interpreted at the protein level based on the finding that TP53(WT) overexpression induced β-catenin protein degradation [41]. However, our study showed that the TP53(WT) genotype is associated with a significant decrease in the β-catenin mRNA level in ovarian cancer cells, suggesting potential alternative crosstalk mechanisms at the transcriptional level. Hyperactivation of WNT signaling in cancer has been found to mediate chemotherapeutic resistance and confer collateral therapeutic vulnerabilities for combination treatment development [55]. A combinatorial effect of WNT pathway inhibitors and taxanes has also been observed in pancreatic, breast and ovarian cancer models [56, 57]. Our studies found a combinatorial effect between WNT pathway inhibitors and paclitaxel in TP53-inactivated ovarian cancer cells. These results indicated that WNT pathway inhibitors could serve as potential chemotherapy adjuvants to improve taxane sensitivity specifically in OC cells with TP53 inactivation.

The association between TP53 inactivation and the taxane resistance phenotype identified in our ovarian cancer cell line models strongly warrants further testing in additional cellular contexts and disease-relevant animal models. Detailed molecular studies on aberrant STING-mediated cell death signaling and WNT/β-catenin signaling in TP53-inactivated OC cells are expected to provide molecular insights into TP53's pluripotent and context-dependent pathophysiological functions.

ACKNOWLEDGEMENTS

This work was supported by the Georgia Research Alliance (Distinguished Investigator award to HF); the NCI Emory Lung Cancer SPORE Career Enhancement Program (P50CA217691 to XM); the Imagine, Innovate and Impact (I^3) Funds from the Emory School of Medicine; and through the Georgia CTSA NIH award (UL1-TR002378) and Winship Cancer Institute (NIH 5P30CA138292). CS is a visiting student in the Emory University School of Medicine-Central South University Xiangya School of Medicine student exchange program. XZ is a visiting student from Zhejiang University School of Medicine. AW is a visiting student in the Emory University School of Medicine-Xi'an Jiaotong University Health Science Center student exchange program.

AUTHOR CONTRIBUTIONS

Conceptualization: CS and HF; In vitro molecular and cellular biology studies: CS, XZ, QN, DC, SD, DF, KQ, XM, and YD; Informatics analysis: AW and AAI; Data analysis: CS, XM, XZ, and HF; Initial manuscript writing: CS, XM, and HF; Funding acquisition, HF; Resources, HF; Supervision, HF. All authors were involved in editing.

ADDITIONAL INFORMATION

Supplementary information The online version contains supplementary material available at https://doi.org/10.1038/s41401-021-00847-6.

Competing interests: The authors declare no competing interests.

REFERENCES

1. Siegel RL, Miller KD, Fuchs HE, Jemal A. Cancer Statistics, 2021. CA Cancer J Clin. 2021;71:7–33.
2. Lheureux S, Braunstein M, Oza AM. Epithelial ovarian cancer: Evolution of management in the era of precision medicine. CA Cancer J Clin. 2019;69:280–304.
3. Ledermann JA, Raja FA, Fotopoulou C, Gonzalez-Martin A, Colombo N, Sessa C, et al. Newly diagnosed and relapsed epithelial ovarian carcinoma: ESMO clinical practice guidelines for diagnosis, treatment and follow-up. Ann Oncol. 2013;24 (Suppl 6):vi24–32.
4. Mikula-Pietrasik J, Witucka A, Pakula M, Uruski P, Begier-Krasinska B, Niklas A, et al. Comprehensive review on how platinum- and taxane-based chemotherapy of ovarian cancer affects biology of normal cells. Cell Mol Life Sci. 2019;76:681–97.
5. McGuire WP, Hoskins WJ, Brady MF, Kucera PR, Partridge EE, Look KY, et al. Cyclophosphamide and cisplatin compared with paclitaxel and cisplatin in patients with stage III and stage IV ovarian cancer. N Engl J Med. 1996;334:1–6.
6. Schiff PB, Fant J, Horwitz SB. Promotion of microtubule assembly in vitro by taxol. Nature. 1979;277:665–7.
7. Horwitz SB. Taxol (paclitaxel): Mechanisms of action. Ann Oncol. 1994;5(Suppl 6): S3–6.
8. Weaver BA. How Taxol/paclitaxel kills cancer cells. Mol Biol Cell. 2014;25:2677–81.
9. Kavallaris M, Kuo DY, Burkhart CA, Regl DL, Norris MD, Haber M, et al. Taxol-resistant epithelial ovarian tumors are associated with altered expression of specific beta-tubulin isotypes. J Clin Invest. 1997;100:1282–93.
10. Orr GA, Verdier-Pinard P, McDaid H, Horwitz SB. Mechanisms of Taxol resistance related to microtubules. Oncogene. 2003;22:7280–95.
11. Dumontet C. Mechanisms of action and resistance to tubulin-binding agents. Expert Opin Investig Drugs. 2000;9:779–88.
12. Cabral F. Factors determining cellular mechanisms of resistance to antimitotic drugs. Drug Resist Updat. 2001;4:3–8.
13. Yin S, Bhattacharya R, Cabral F. Human mutations that confer paclitaxel resistance. Mol Cancer Ther. 2010;9:327–35.
14. Dumontet C, Sikic BI. Mechanisms of action of and resistance to antitubulin agents: microtubule dynamics, drug transport, and cell death. J Clin Oncol. 1999;17:1061–70.
15. Gottesman MM. Mechanisms of cancer drug resistance. Annu Rev Med. 2002;53:615–27.
16. Kastenhuber ER, Lowe SW. Putting p53 in context. Cell. 2017;170:1062–78.
17. Levine AJ. p53, the cellular gatekeeper for growth and division. Cell. 1997;88:323–31.
18. Marks JR, Davidoff AM, Kerns BJ, Humphrey PA, Pence JC, Dodge RK, et al. Overexpression and mutation of p53 in epithelial ovarian cancer. Cancer Res. 1991;51:2979–84.
19. Wahl AF, Donaldson KL, Fairchild C, Lee FY, Foster SA, Demers GW, et al. Loss of normal p53 function confers sensitization to Taxol by increasing G2/M arrest and apoptosis. Nat Med. 1996;2:72–9.
20. Debernardis D, Sire EG, De Feudis P, Vikhanskaya F, Valenti M, Russo P, et al. p53 status does not affect sensitivity of human ovarian cancer cell lines to paclitaxel. Cancer Res. 1997;57:870–4.
21. Lanni JS, Lowe SW, Licitra EJ, Liu JO, Jacks T. p53-independent apoptosis induced by paclitaxel through an indirect mechanism. Proc Natl Acad Sci USA. 1997;94:9679–83.
22. Vikhanskaya F, Vignati S, Beccaglia P, Ottoboni C, Russo P, D'Incalci M, et al. Inactivation of p53 in a human ovarian cancer cell line increases the sensitivity to paclitaxel by inducing G2/M arrest and apoptosis. Exp Cell Res. 1998;241:96–101.
23. Guntur VP, Waldrep JC, Guo JJ, Selting K, Dhand R. Increasing p53 protein sensitizes non-small cell lung cancer to paclitaxel and cisplatin in vitro. Anticancer Res. 2010;30:3557–64.
24. Parmakhtiar B, Burger RA, Kim JH, Fruehauf JP. HIF Inactivation of p53 in ovarian cancer can be reversed by topotecan, restoring cisplatin and paclitaxel sensitivity. Mol Cancer Res. 2019;17:1675–86.
25. Seagle BL, Yang CP, Eng KH, Dandapani M, Odunsi-Akanji O, Goldberg GL, et al. TP53 hot spot mutations in ovarian cancer: Selective resistance to microtubule stabilizers in vitro and differential survival outcomes from The Cancer Genome Atlas. Gynecol Oncol. 2015;138:159–64.
26. Alafate W, Li X, Zuo J, Zhang H, Xiang J, Wu W, et al. Elevation of CXCL1 indicates poor prognosis and radioresistance by inducing mesenchymal transition in glioblastoma. CNS Neurosci Ther. 2020;26:475–85.
27. Tang C, Mo X, Niu Q, Wahafu A, Yang X, Qui M, et al. Hypomorph mutation-directed small-molecule protein-protein interaction inducers to restore mutant SMAD4-suppressed TGF-beta signaling. Cell Chem Biol. 2021;28:636–47 e5.
28. Rees MG, Seashore-Ludlow B, Cheah JH, Adams DJ, Price EV, Gill S, et al. Correlating chemical sensitivity and basal gene expression reveals mechanism of action. Nat Chem Biol. 2016;12:109–16.

29. Li Z, Ivanov AA, Su R, Gonzalez-Pecchi V, Qi Q, Liu S, et al. The OncoPPi network of cancer-focused protein-protein interactions to inform biological insights and therapeutic strategies. Nat Commun. 2017;8:14356.
30. Kotla S, Peng T, Bumgarner RE, Gustin KE. Attenuation of the type I interferon response in cells infected with human rhinovirus. Virology. 2008;374:399–410.
31. Zhou Y, Zhou B, Pache L, Chang M, Khodabakhshi AH, Tanaseichuk O, et al. Metascape provides a biologist-oriented resource for the analysis of systems-level datasets. Nat Commun. 2019;10:1523.
32. Mo X, Tang C, Niu Q, Ma T, Du Y, Fu H. HTiP: High-throughput immunomodulator phenotypic screening platform to reveal IAP antagonists as anti-cancer immune enhancers. Cell Chem Biol. 2019;26:331–9 e3.
33. Guzman C, Bagga M, Kaur A, Westermarck J, Abankwa D. ColonyArea: an ImageJ plugin to automatically quantify colony formation in clonogenic assays. PLoS One. 2014;9:e92444.
34. Vasey PA, Jayson GC, Gordon A, Gabra H, Coleman R, Atkinson R, et al. Phase III randomized trial of docetaxel-carboplatin versus paclitaxel-carboplatin as first-line chemotherapy for ovarian carcinoma. J Natl Cancer Inst. 2004;96:1682–91.
35. Agarwal R, Kaye SB. Ovarian cancer: Strategies for overcoming resistance to chemotherapy. Nat Rev Cancer. 2003;3:502–16.
36. Lohard S, Bourgeois N, Maillet L, Gautier F, Fetiveau A, Lasla H, et al. STING-dependent paracriny shapes apoptotic priming of breast tumors in response to anti-mitotic treatment. Nat Commun. 2020;11:259.
37. Aubrey BJ, Kelly GL, Janic A, Herold MJ, Strasser A. How does p53 induce apoptosis and how does this relate to p53-mediated tumour suppression? Cell Death Differ. 2018;25:104–13.
38. Farnebo M, Bykov VJ, Wiman KG. The p53 tumor suppressor: A master regulator of diverse cellular processes and therapeutic target in cancer. Biochem Biophys Res Commun. 2010;396:85–9.
39. Wang TH, Wang HS, Soong YK. Paclitaxel-induced cell death: Where the cell cycle and apoptosis come together. Cancer. 2000;88:2619–28.
40. Jung YS, Park JI. Wnt signaling in cancer: Therapeutic targeting of Wnt signaling beyond beta-catenin and the destruction complex. Exp Mol Med. 2020;52:183–91.
41. Sadot E, Geiger B, Oren M, Ben-Ze'ev A. Down-regulation of beta-catenin by activated p53. Mol Cell Biol. 2001;21:6768–81.
42. Wellenstein MD, Coffelt SB, Duits DEM, van Miltenburg MH, Slagter M, de Rink I, et al. Loss of p53 triggers WNT-dependent systemic inflammation to drive breast cancer metastasis. Nature. 2019;572:538–42.
43. Nguyen VHL, Hough R, Bernaudo S, Peng C. Wnt/beta-catenin signalling in ovarian cancer: Insights into its hyperactivation and function in tumorigenesis. J Ovarian Res. 2019;12:122.
44. Zhan T, Rindtorff N, Boutros M. Wnt signaling in cancer. Oncogene. 2017;36:1461–73.
45. Emami KH, Nguyen C, Ma H, Kim DH, Jeong KW, Eguchi M, et al. A small molecule inhibitor of beta-catenin/CREB-binding protein transcription [corrected]. Proc Natl Acad Sci USA. 2004;101:12682–7.
46. Huang SM, Mishina YM, Liu S, Cheung A, Stegmeier F, Michaud GA, et al. Tankyrase inhibition stabilizes axin and antagonizes Wnt signalling. Nature. 2009;461:614–20.
47. Chu Q, Vincent M, Logan D, Mackay JA, Evans WK. Lung cancer disease site group of cancer care Ontario's program in evidence-based C. Taxanes as first-line therapy for advanced non-small cell lung cancer: a systematic review and practice guideline. Lung Cancer. 2005;50:355–74.
48. Schmid P, Adams S, Rugo HS, Schneeweiss A, Barrios CH, Iwata H, et al. Atezolizumab and nab-paclitaxel in advanced triple-negative breast cancer. N Engl J Med. 2018;379:2108–21.
49. Freeman JA, Espinosa JM. The impact of post-transcriptional regulation in the p53 network. Brief Funct Genomics. 2013;12:46–57.
50. Kitayner M, Rozenberg H, Kessler N, Rabinovich D, Shaulov L, Haran TE, et al. Structural basis of DNA recognition by p53 tetramers. Mol Cell. 2006;22:741–53.
51. Wei CL, Wu Q, Vega VB, Chiu KP, Ng P, Zhang T, et al. A global map of p53 transcription-factor binding sites in the human genome. Cell. 2006;124:207–19.
52. Fujino T, Kang MJ, Suzuki H, Iijima H, Yamamoto T. Molecular characterization and expression of rat acyl-CoA synthetase 3. J Biol Chem. 1996;271:16748–52.
53. Yan L, He Z, Li W, Liu N, Gao S. The Overexpression of Acyl-CoA Medium-Chain Synthetase-3 (ACSM3) suppresses the ovarian cancer progression via the inhibition of integrin beta1/AKT signaling pathway. Front Oncol. 2021;11:644840.
54. Ruan HY, Yang C, Tao XM, He J, Wang T, Wang H, et al. Downregulation of ACSM3 promotes metastasis and predicts poor prognosis in hepatocellular carcinoma. Am J Cancer Res. 2017;7:543–53.
55. Mohammed MK, Shao C, Wang J, Wei Q, Wang X, Collier Z, et al. Wnt/beta-catenin signaling plays an ever-expanding role in stem cell self-renewal, tumorigenesis and cancer chemoresistance. Genes Dis. 2016;3:11–40.
56. Fischer MM, Cancilla B, Yeung VP, Cattaruzza F, Chartier C, Murriel CL, et al. WNT antagonists exhibit unique combinatorial antitumor activity with taxanes by potentiating mitotic cell death. Sci Adv. 2017;3:e1700090.
57. Shetti D, Zhang B, Fan C, Mo C, Lee BH, Wei K. Low dose of paclitaxel combined with XAV939 attenuates metastasis, angiogenesis and growth in breast cancer by suppressing Wnt Signaling. Cells. 2019;8:892.